Hanaor, D. A. H. *et al*. (2016). *Géotechnique* **66**, No. 4, 323–332 [http://dx.doi.org/10.1680/jgeot.15.P.034]

3D printable geomaterials

D. A. H. HANAOR*, Y. GAN*, M. REVAY*, D. W. AIREY* and I. EINAV*

One of the many attributes of three-dimensional (3D) printing is the ability to produce particles with independent control of morphology and material properties, parameters that are inexorably entwined in naturally occurring geomaterials. In this paper the 3D printing of surrogate granular materials is described, with examples of the particles produced, and results are presented showing their ability to capture real soil behaviour. Three approaches are demonstrated for the 3D generation of model grains. The first method involves the superimposition of a fractal surface with higher level stochastic features on the face of a closed volume, such as a geodesic spheroid. The second method involves the use of Fourier descriptors or fractal geometry generated from two-dimensional (2D) cross-sections and their interpolation to produce simulated geomaterial particles in three dimensions. The third method involves the generation of complex particles by the aggregation of polyhedral elements such as cubes or octahedra which is suitable for the simulation and fabrication of porous or branching particles. Triaxial tests have been performed on particles produced by the second method, which most readily allows input parameters to be obtained from natural geomaterials. Results of these tests show the ability of the printed particles to reproduce soil behaviour, and demonstrate the effect of particle shape on the material response. Finally, applications of the fabrication of surrogate materials by 3D printing are discussed, for use as standardised, printable geomaterials in future up-scaled geotechnical experiments and other geomechanical research.

KEYWORDS: gravels; laboratory tests; model tests; particle-scale behaviour; sands

INTRODUCTION

Understanding the micromechanical origins of the behaviour of granular materials is of increasing interest across multiple disciplines in science and engineering. In a broad range of naturally occurring granular materials, including soils, sediment particles, sand rocks and minerals, there is a need to establish better relationships between the multi-scale particle morphology of these geomaterials and their mechanical, hydrological and rheological performance. This has the potential to enable more efficient utilisation of natural resources and improved reliability in geotechnical and environmental applications (Scheel *et al.*, 2008; Salot *et al.*, 2009). Recent years have seen increasing research efforts aimed at gaining new insights into such relationships through computational and experimental methods (Cho *et al.*, 2006; Cavarretta *et al.*, 2010; Brisard *et al.*, 2012; Mollon & Zhao, 2013b).

The utility and significance of three-dimensional (3D) printing techniques for the analysis of granular morphology was demonstrated recently in a study by Miskin & Jaeger (2013). In this study idealised printed grains were constructed by joining one to four spherical units with minimal overlaps. Improvements in the capabilities and cost-effectiveness of 3D printing technologies, combined with the availability of computational resources that permit high-resolution simulations, have made it possible to produce grain morphologies representative of real geomaterial particles in large quantities. Furthermore, the range of materials has expanded, facilitating the fabrication of complex grains with fixed morphology for different material properties. These capabilities now allow independent control of morphology and material properties.

Manuscript received 17 February 2015; revised manuscript accepted 12 October 2015. Published online ahead of print 4 December 2015. Discussion on this paper closes on 1 September 2016, for further details see p. ii.

* School of Civil Engineering, University of Sydney, Sydney, NSW, Australia

The simulation of realistic geomaterial grain morphologies is of value not only in 3D printing but also for discrete-element method (DEM) models of granular materials (Matsushima *et al.*, 2003). Such methods have often assumed simplified geometries, such as spherical or circular elements (Cundall & Strack, 1979; Persson & Frenning, 2012), clustered spheres or discs (Thomas & Bray, 1999), polygons (Alonso-Marroquín *et al.*, 2008) or sphero-polygons (Alonso-Marroquin, 2008; Alonso-Marroquín & Wang, 2009) and polyhedra (Langston *et al.*, 2013). Although these simplified geometries may be utilised effectively on a case-by-case basis, the hierarchical origins of surface-localised physical behaviour in geomaterials means that more complex approaches are necessary for the purposes of describing, predicting or explaining the morphological dependence of these characteristics (Alonso-Marroquín *et al.*, 2013; Hanaor *et al.*, 2013).

In naturally occurring geomaterials, macroscopically observed properties of friction and contact stiffness between grains are, in addition to bulk properties, governed by surface structures, which exhibit self-affine geometries showing features across a range of length scales (Hanaor *et al.*, 2014; Russel, 2014). Surface structures of granular material can be considered as an extension of hierarchical morphology exhibiting non-integer dimensionality (Arasan *et al.*, 2011; Qin *et al.*, 2013). Additionally, cohesion and capillary forces between grains are also governed by surface structures (Fraysse *et al.*, 1999), further motivating the development of methods to characterise and model natural grain morphologies.

Methods to describe and classify the morphologies of naturally occurring grains predominantly invoke measures of sphericity, roundness, convexity and roughness. These parameters have been defined in a variety of manners, and have been the subject of many reviews (Barrett, 1980; Pourghahramani & Forssberg, 2005; Blott & Pye, 2008). Charts put forward by Krumbein and Sloss have frequently

been employed for the conventional classification of geomaterials over the past six decades (Krumbein & Sloss, 1951). However, the use of these morphological descriptors is driven primarily by convenience rather than physical meaning. Geomaterial grains are not uniquely defined by this type of descriptor and, although these parameters can be extracted from image analysis with ever increasing ease (Liao *et al.*, 2010; Altuhafi *et al.*, 2012), they are insufficient for the computational generation and printing of simulated geomaterial particles.

Recent years have seen a growing interest in utilising Fourier descriptors (FDs) to characterise particle shape on the basis of planar grain projections. This approach was first put forward in 1970 (Ehrlich & Weinberg, 1970) and utilises the Fourier spectrum of two-dimensional (2D) contours to characterise grain morphology in terms of a series of numerical descriptors (Thomas *et al.*, 1995; Bowman *et al.*, 2001). The notable advantage to the use of FDs is their applicability in grain simulation procedures as pioneered by Mollon and Zhao over recent years (Mollon & Zhao, 2012, 2013a).

The ability to print surrogate granular material opens the door to new research methodologies that can assist in establishing the micromechanical origins, and the role of morphology and material properties, in the behaviour of granular materials. Importantly, the concept of printable granular geomaterials offers an avenue to 'standardise' soil for quality control and calibration in geotechnical testing. Currently standard materials in geotechnical laboratories are mineral sands and soils from particular geological sources, for example, Ottawa sands (Tarnawski *et al.*, 2009). This limitation could be overcome if the ability to fabricate uniform and consistent geomaterial specimens with controlled standardised properties could be attained.

In order to realise the opportunities afforded by 3D printing techniques in the study of granular materials, two identifiable criteria must be met: (*a*) simulated granular matter must be meaningful and realistic representations of the materials of interest; and (*b*) parameters utilised in the generation of simulated granular matter should be readily acquirable from real materials.

In this paper, methods are presented and discussed for the 3D simulation of realistic granular materials for application in 3D printing of standardised surrogate geomaterials, and show examples of the 3D printed particles produced. Results are further presented showing the ability of a bulk quantity of the printable material to capture real sand behaviour under drained triaxial loading conditions, and issues relating to the utilisation of these methods in the study of micromechanical interactions in granular materials are examined.

MATERIALS AND METHODOLOGY

For the different approaches presently reported, simulated grains were generated in a Matlab environment and, with all methods, individual grains were described by discrete sets of corresponding vertices and faces. Additionally, subsequent to scaling, single grains or sets of multiple grains were converted into a standard tessellation language (STL) format suitable for visualisation by computed aided design (CAD) software and for fabrication by 3D printing methods. Using these methods, grains can be generated in alternative computational environments and alternate output formats can be used. Fabrication of the grains reported here was carried out using layer-by-layer photo-polymerisation by means of an Objet Eden 250 poly-jet type 3D printer with a manufacturer stated resolution of 4 μm and 32 μm in the horizontal and vertical directions, respectively, using Fullcure 720 resin (Stratasys, USA) in a layer-by-layer printing method. The cured polymer has a specific gravity of 1·19 (confirmed by following standard testing procedure) and an elastic modulus of 2·87 GPa. It may be noted that these properties differ significantly from the values of Gs, 2·64 and elastic modulus, ~90 GPa typically found for quartz.

Method 1: fractal surface overlay (FSO)

Natural materials in general, and geomaterials in particular, often exhibit multi-scale surface structures featuring statistical self-similarity or fractality (Brantley *et al.*, 1999; Babadagli & Develi, 2003; Buzio *et al.*, 2003). For interfaces this fractality is quantified by reference to macroscopically flat surfaces. The same approach can be applied to define the morphology of grains by their interface structure across multiple scales overlaid on a spheroidal or polygonal macrostructure.

The Ausloos–Berman type variants of the Weierstrass Mandelbrot function are used for the generation of fractal surfaces with stochastic highest level features. In macroscopically flat surfaces this can be used for the simulation of realistic surfaces. In such macroscopically planar surfaces the surface height function can be described in polar coordinates (ρ, θ) in the following form (Ausloos & Berman, 1985; Yan & Komvopoulos, 1998; Ciavarella *et al.*, 2008; Komvopoulos, 2008; Hanaor *et al.*, 2015)

$$Z(\rho,\ \theta) = \sqrt{\frac{\ln\ \gamma}{M}} \sum_{m=1}^{M} \sum_{n=0}^{n\ \max} \left(\frac{2\pi\gamma^n}{L}\right)^{D-3} \times \left\{\cos\psi_{m,n} - \cos\left[\frac{2\pi\gamma^n}{L}\rho\ \cos\ (\theta - \alpha_m) + \psi_{m,n}\right]\right\} \tag{1}$$

Here n corresponds to consecutive frequency exponents and, as with previous work, in this approach M and $n_{\max}$ define the number of superimposed ridges and frequencies used to construct the surface and it was found that a value of $M = n_{\max} = 40$ gives a sufficiently random surface structure, such that parallel ridge networks are absent, as observed in the present and prior work (Hanaor *et al.*, 2013). γ corresponds to a scaling factor relating to the density of frequencies used to construct the surface and is set at 1·5, similarly to previous work (Yan & Komvopoulos, 1998; Ciavarella *et al.*, 2006); α_m is an arbitrary angle used to offset asperity ridges in the azimuthal direction; D is the fractal dimension; and L is a stochastic length parameter.

In applying this method to the simulation of grain surfaces, varying L at lower values allows for the control of the nodularity (the number of highest scale nodes protruding from the grain), whereas varying L at higher values (greater than half of the circumference) allows for the control of grain elongation, using a variant of equation (1). To implement this, a geodesic sphere is simulated at a desired resolution on the basis of an icosahedral primitive unit to yield evenly distributed $(\theta,\ \phi)$ pairs where θ [0 2π] is the coordinate azimuth and ϕ [0 π] is the elevation. The vectors representing the surface coordinates are adjusted to give a fractal surface structure overlaid on the geodesic sphere. This is done separately for the two hemispheres to avoid symmetry about the equator. For vertices in the first hemisphere, having $\phi \leq \pi/2$, sphere radii are adjusted in the following form

$$R_1(\theta,\phi) = R_0 + K \sum_{m=1}^{M} \sum_{n=1}^{n\max} \left(\frac{2\pi\gamma^{n-1}}{L}\right)^{D-3} \left\{\cos(\psi_{m,n} + \zeta_{m,n}\cos\phi) - \cos\left[\frac{2\pi\phi\gamma^n}{L}\cos(\theta - \alpha_m) + \psi_{m,n} + \zeta_{m,n}\ \cos\phi\right]\right\} \tag{2}$$

where R_0 is the radius of the initial geodesic spheroid, ψ is a random phase angle and K is an amplitude scaling parameter. For coordinates in the second hemisphere, having values of $\phi > \pi/2$, radii are adjusted as follows

$$R_2(\theta,\phi) = R_0 + K\sum_{m=1}^{M}\sum_{n=1}^{n\max}\left(\frac{2\pi\gamma^{n-1}}{L}\right)^{D-3}\left\{\cos\psi_{m,n} - \cos\left[\frac{2\pi(\pi-\phi)\gamma^n}{L}\cos(\theta-\alpha_m)+\psi_{m,n}\right]\right\} \quad (3)$$

To impart surface structure randomness, a set of randomised phase angles ψ of the size $M \times n_{\max}$ is included, given by a uniform distribution $\psi_{m,n} = U(0, 2\pi)$. To avoid symmetry, for the surface of the lower hemisphere where $\phi \leq \pi/2$, a second phase angle ζ is included and multiplied by the term $\cos\phi$ to give continuity of the surface across the equator (where $\phi = \pi/2$). A scaling factor K is included in order to normalise the amplitude of the surface features to a desired level relative to the initial geodesic spheroid radius R_0.

The results of this grain generation method and the effects of varying the stochastic length parameter are shown in Fig. 1. By varying the proportional size of L relative to the grain radius, it is possible to create grains with a varying number of highest level features which can yield oblong, nodular or rough grain morphologies, as shown. It can be seen that low L/R values tend to yield unrealistic grains exhibiting a large number of protrusions.

For a given value of L/R, the fractal dimension D can be varied to yield controlled surface-structure scaling behaviour, illustrated in Fig. 2. As with the stochastic length parameter, excessively high or low fractality values lead to unrealistic grain structures in the simulated geomaterials.

In the present work the precursor shape from which grains are created is a geodesic sphere. However, equivalent methodologies can be implemented using geodesic precursors generated by 3D Voronoi tessellation or other methods similar to previously reported approaches (Pena *et al.*, 2007; Mollon & Zhao, 2012, 2014). By adjusting the magnitude of the barycentric vectors of the primitive geodesic object, particle morphologies are generated such that all rays emanating from a central point within the particle intersect the particle surface exactly once. Such morphologies are also referred to as star-like (Robertson, 1936; Natalini *et al.*, 2008). While generation of particles with fractal surface overlays allows a wide range of shapes to be generated, acquiring appropriate input parameters from natural geomaterials through morphological analyses is difficult owing to the complexity of meaningful multi-scale surface analysis.

Method 2: contour rotation interpolation (CRI)

The morphological characterisation of granular materials using image processing based methods, with initial data acquired through electron microscopy or optical methods, frequently yields 2D grain contours or polyhedra as output. These geometries describe planar projections of grains, as described by Cartesian or polar coordinates. Additionally, the computational simulation of geomaterial morphology is often conducted towards the generation of such 2D geometries owing to the greater speed with which such algorithms can be implemented relative to 3D grain generation.

A novel computational method for generating realistic 3D grain morphologies on the basis of the interpolation of three 2D grain contours was first developed and reported in a recent publication by Mollon and Zhao, and has been described in greater detail elsewhere (Mollon & Zhao, 2012, 2013a, 2014). Generating particles by CRI relies in principle on the generation of three closed grain cross-sections, like those shown in Fig. 3, followed by processes of contour correction, revolution, stretching and morphing in order to render a morphology that amalgamates the three grain projections into a single 3D object. A variety of methods can be used to obtain realistic grain sections. Fig. 3 shows examples generated by a fractal surface profile, FDs and from a sand grain micrograph.

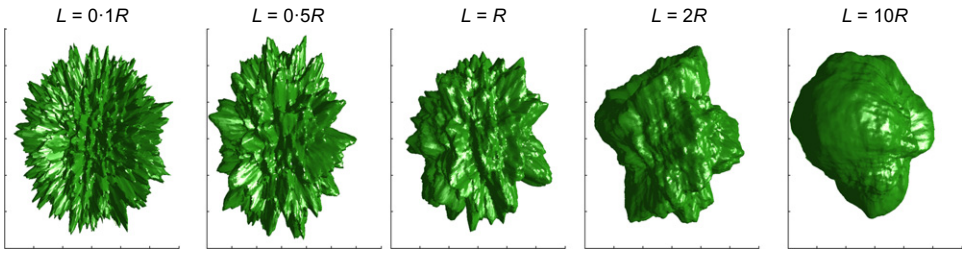

Fig. 1. Grains simulated using the FSO method with the stochastic length parameter (L) varied relative to grain radius from 0·1R to 10R. Fractal dimension is maintained constant at 2·4

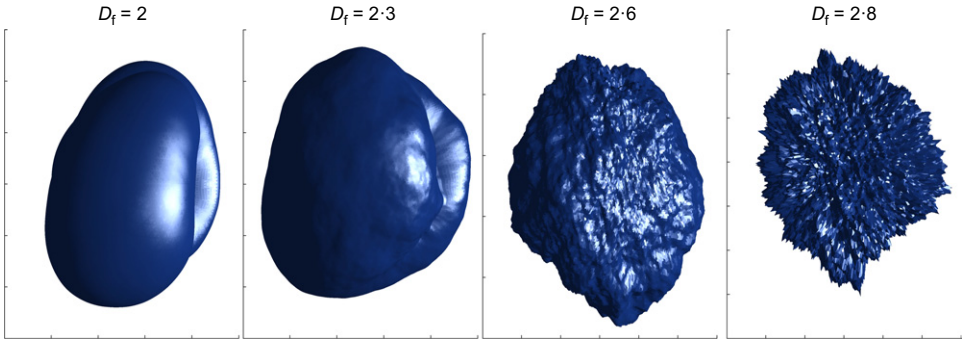

Fig. 2. Grains simulated using the FSO method with the applied fractal dimension (D) varied from 2 to 2·8. Stochastic length parameter is constant at $L = 7R$

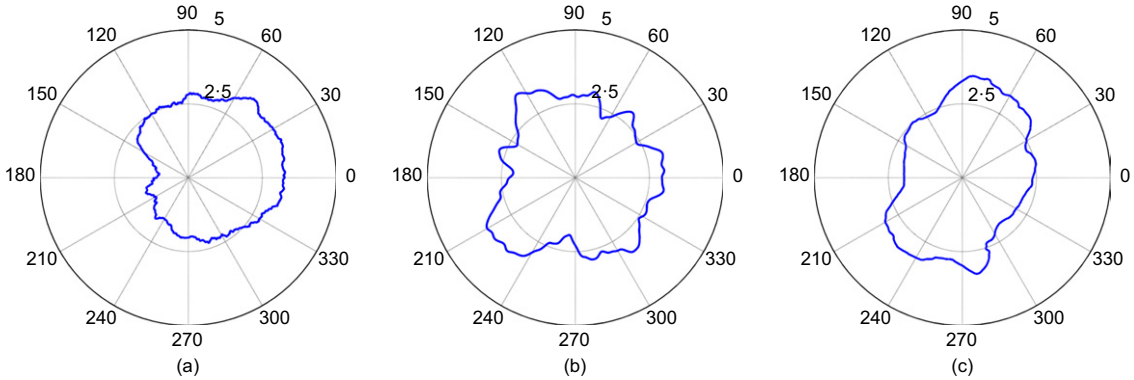

Fig. 3. Sample grain contours from three sources: (a) a simulated fractal grain profile, (b) FD-based contour simulation and (c) a grain micrograph obtained by optical microscopy

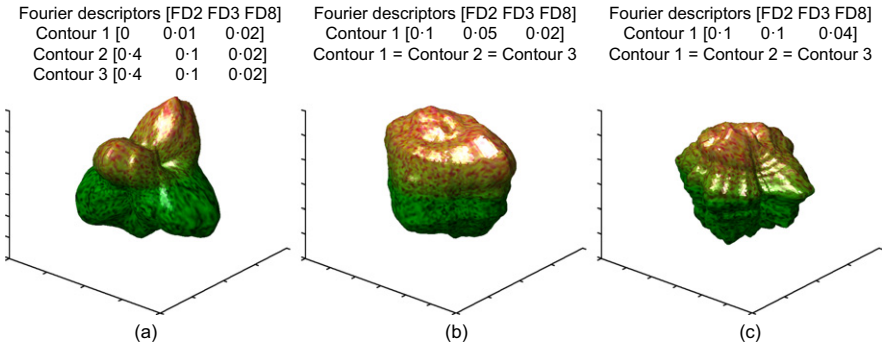

Fig. 4. Sample grains simulated by the CRI method using FD-derived contours

This method generates 3D geometries where each surface point is defined by a distinct coordinate (ρ, θ, φ). Thus, as with grain generation by FSO, this method yields star-like objects and does not allow for the generation of branching or porous morphologies.

On the basis of Mollon and Zhao's methods, contours can be generated by means of a Fourier construction, with the modes of the amplitude spectrum, known as Fourier descriptors (FDs). Fourier descriptors 2, 3 and 8 have been shown to respectively relate to characteristics of elongation, irregularity and roughness, while the remaining descriptors are calculated following an assumed regression (Mollon & Zhao, 2012). In order to generate a realistic population of non-uniform particles, a randomised set of phase angles, generated in Matlab, is included to decompose the FDs into the elements of the Fourier spectrum, which can then be used to generate a unique grain contour, such as that shown in Fig. 3(b). The construction of a 3D grain by CRI of FD-based contours can utilise contours generated with a constant set of descriptors, or may utilise three contours, each of which is generated using divergent descriptors, to account for anisotropy effects.

It is important to note that these descriptors can be derived from the Fourier transform of the 2D grain contours, which can be obtained from the analysis of grain micrographs by scanning electron microscopy (SEM) or optical microscopy, such as that shown in Fig. 3(c).

Additionally, CRI based grain generation can be carried out using fractal surface profiles as input 2D contours. These contours, such as the one shown in Fig. 3(a), can be generated by adjusting radii of a circle following 2D variants of equation (1), where θ is held constant.

The integration of three scaled grain contours following the interpolation procedure of Mollon and Zhao results in the simulation of 3D grains such as those shown in Fig. 4. This figure shows grains, each of which was generated from three FD-defined contours. In Fig. 4(a) contours are generated from three different FD sets, whereas in Figs 4(b) and 4(c) all three contours are generated using the same FD set. The grains thus produced exhibit irregularity typical of natural particles; however, the interpolation method currently employed yields some unrealistic parallel ridges.

Method 3: directed polyhedra aggregation (DPA)

Naturally occurring geomaterials occasionally exhibit morphologies that are not star-like or fully dense and thus cannot be described by a unique set of (ρ, θ, ϕ) coordinates. In soils, sediments, organic matter and precipitates, branching and porous forms are often encountered as the result of growth and aggregation processes; the morphologies of these particles, which can be described as fractal structures, are of growing interest in numerous applications (Tang *et al.*, 2002; Gastaldi & Vanni, 2011; Hanaor *et al.*, 2014). The ability to meaningfully simulate this type of particle is of value in enabling the study of the morphological dependence of hydrodynamics, mechanics, interfacial interactions and transport phenomena in granular media dominated by non-star-like particles (surface points are not described by a unique set of vectors). Additionally, tools for the simulation of porous and/or branching aggregates are of value for the study of particle formation in processes of aggregation, precipitation and agglomeration and the dependence of these processes on environmental conditions and system parameters (e.g. pH, temperature or surface charge).

In contrast to methods, such as FSO and CRI, that generate particles by varying the surface structure of initial primitive geodesic spheroids or Voronoi type cells, the DPA method employs an aggregation algorithm to construct particles of varied porosity and volume fractality from many

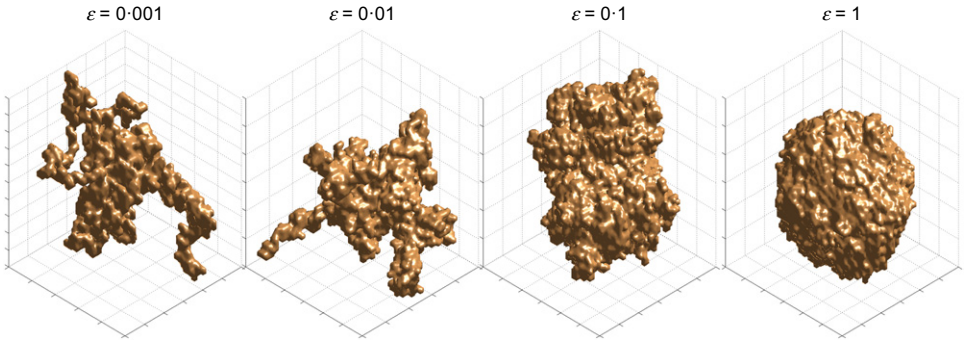

Fig. 5. Grains simulated using the DPA method with cubes, showing varied values of the exponent ε resulting in particles with controllable fractality

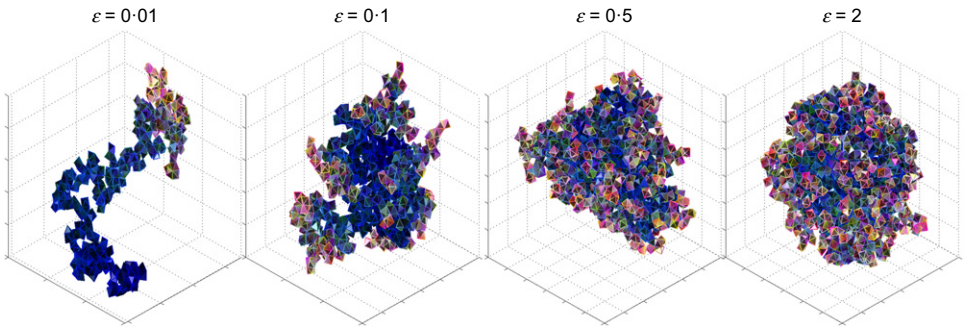

Fig. 6. Grains simulated using the DPA method with octahedra, showing varied values of the exponent ε resulting in particles with controllable fractality

convex polyhedral primary particles. Comparable algorithms for the simulation of 3D and 2D aggregates from spheroidal and cubic primary particles have been reported in earlier works (Erlebacher *et al.*, 1993; Maggi & Winterwerp, 2004; Schmid *et al.*, 2004).

In the presently reported DPA method the morphology of aggregate geomaterial particles was controlled using Matlab by the probability for the nth primary particle to attach to an existing polyhedron with index i ($1 \leq i \leq n-1$) with respect to the history of primary particle addition, where $n-1$ is the existing number of primary particles. Thus, the probability that an existing particle with index $a \leq i \leq b$ is chosen to receive a newly placed nth primary polyhedral particle is

$$\Pr[a \leq i \leq b] = \left(\frac{\varepsilon}{n-1^{\varepsilon}} \int_{a-1}^{b} i^{\varepsilon-1} \mathrm{d}i \right) \tag{4}$$

The nth primary particle, described by face/vertex data, is then added to one of the unoccupied faces of primary particle i. The probability $\Pr[a \leq i \leq b]$ is a function of the exponent ε; low exponent values result in preferential addition onto older primary particles yielding closed sphere-like aggregates, with little or no porosity (zero volume porosity is only possible when primary particles are cubic); high exponent values result in preferential addition of primary particles onto faces of recently added particles, which are likely to be away from the aggregated centre of mass yielding branching aggregates. This approach is readily achieved in a Matlab environment by applying the exponent ε to a uniformly distributed pseudorandom selection from existing indices.

The techniques explored here can be applied using various Platonic polyhedral elements (geometries where all faces are identical polygons) or Archimedean polyhedra (faces are of two or more types of regular polygon meeting at identical vertices) (Torquato & Jiao, 2009a). In the present work, the application of this method is demonstrated using cubic and octahedral primary particles, shown respectively in Fig. 5 and Fig. 6. Smoothing of sharp corners can be carried out by interpolation of the face-vertex data as illustrated for the aggregates shown in Fig. 5. For the case of aggregation of octahedral primary particles, illustrated in Fig. 6, in addition to the selection of a face on which to attach each new particle, the aggregation algorithm includes a step to select one of three possible rotational orientations for the newly attached octahedron. Moreover, while cubic aggregation occurs in a regular lattice, where sites are either occupied or vacant, for construction from octahedral elements, a further step is necessary to ensure that no intrusion into existing particles occurs. The simulation of fully dense aggregates is only possible with cubic elements, as other Platonic or Archimedean solids do not allow fully dense spatial tiling (Torquato & Jiao, 2009a, 2009b). The use of octahedral or other non-cubic elements yields more porous aggregates even at high exponent values.

RESULTS

Particle simulation and fabrication

The morphologies obtained by the three methods can be fabricated using 3D printing methods and are further utilisable in DEM models. Here the 3D printer output from the poly-jet fabrication of particles is shown alongside computer renderings of the morphologies.

Figure 7 shows the results of the 3D printing based fabrication of simulated grains generated by the FSO method. All features present in the simulated grain object are captured by the fabrication process employed. With less regular, smaller-scale features some distortion is found to occur about the grain equator for grains where the amplitude of roughness

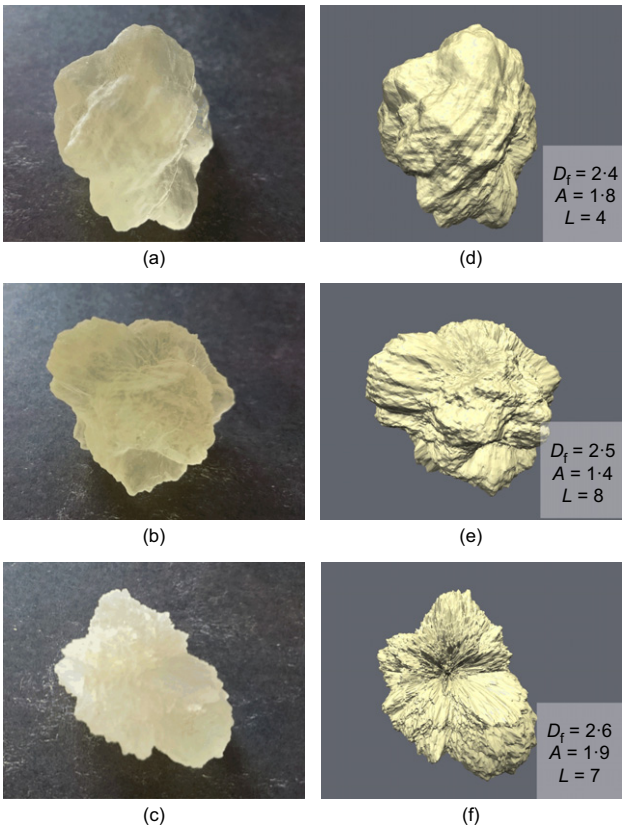

Fig. 7. Comparison of printed (a), (b), (c) and simulated grains (d), (e), (f) obtained by the FSO method

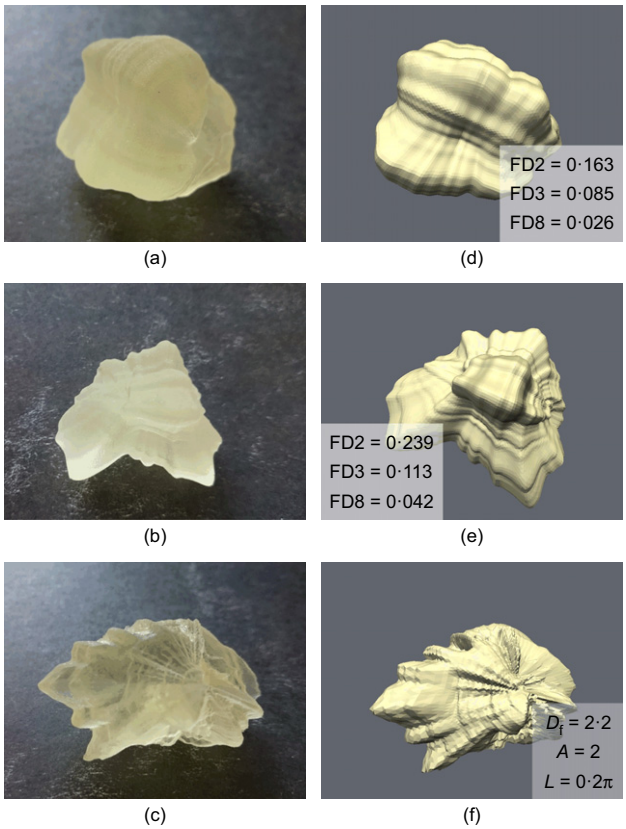

Fig. 8. Comparison of printed (a), (b), (c) and simulated grains (d), (e), (f) obtained by the CRI method

features is large relative to the grain radius. The generation of realistic surface morphologies necessitates the use of appropriate parameters of fractal dimension (D), stochastic length scale (L) and amplitude scaling (K) in the application of equations (2) and (3). Simulated grains can be obtained using the FSO method with similitude to many rock and sand geomaterial particles in traditional terms of sphericity, surface roughness, convexity/concavity and elongation. However, anisotropic roughness, faceted surface regions, open pores and angular vertices are not achievable with this approach. Furthermore, this approach is unsuitable for geomaterials that do not exhibit multi-scale features, such as angular grains with smooth surfaces.

Grains simulated and fabricated using the CRI approach are shown in Fig. 8. Similarly to previously reported results obtained from this method, grains show anisotropic features in the form of tangentially parallel surface ridges. As with the FSO method this approach shares the disadvantage of not being able to readily facilitate the generation of grains with faceted regions and/or angular vertices, frequently encountered in natural geomaterial systems. Figures 8(a) and 8(d) were generated on the basis of the mean FDs extracted from the morphological characterisation of over 1700 grains of quartz sand. On the basis of the projections of these grains, this sand was found to have mean aspect ratio 0·766, mean circularity 0·863 and mean convexity of 0·986, where circularity refers to the ratio of the circumference of equivalent-area circles to the actual perimeters of particle projections and convexity describes the ratio of particle convex hull perimeters to actual perimeters. Similarly, Figs 8(b) and 8(e) were obtained on the basis of the mean FDs extracted from the morphological characterisation of over 2500 grains of garnet sand. On the basis of the projections of these grains, this sand was found to have mean aspect ratio 0·640, mean circularity 0·722 and mean convexity of 0·979. Figures 8(c) and 8(f) show the CRI generated grain on the basis of 2D contours defined by fractal surface profiles. Examination of these objects shows that the particles produced are not representative of the original material, lacking facets and angularity, and further suggests that the implementation of fractal surface structure generation is more appropriately carried out using methods of the FSO type. It should be noted that more recent published studies applying random field theory on a 3D grain surface have been shown to facilitate the application of grain FDs to generate more realistic grains featuring faceted geometries without the occurrence of parallel surface ridges (Mollon & Zhao, 2014).

Computer rendered and printed aggregate particles generated by the DPA methods described here are shown in Fig. 9. While a wide range of realistic aggregate particles are obtainable from these methods, printed specimens exhibiting a highly branching or fractal structure are found to be fragile, particularly if a small primary particle size is employed.

The morphologies that can be generated by DPA algorithms are applicable in the study of fractal aggregates such as the type often encountered in sedimentology. By constructing a calibration curve, it is possible to control the value of the exponent ε to yield a desired aggregate fractal dimension (D_A), which corresponds to a term of the type

$$D_A = \frac{\log\ V}{\log\ A} \tag{5}$$

where V corresponds to the true particle volume and A relates to the mean linear size of the smallest bounding box possible.

The evaluation of the fractality of aggregate particles in air, soils or aqueous media and the study of the physical and mechanical behaviour of such materials in a range of applications have motivated numerous studies in recent years (Tang *et al.*, 2001, 2002, 2003; Tang & Raper, 2002;

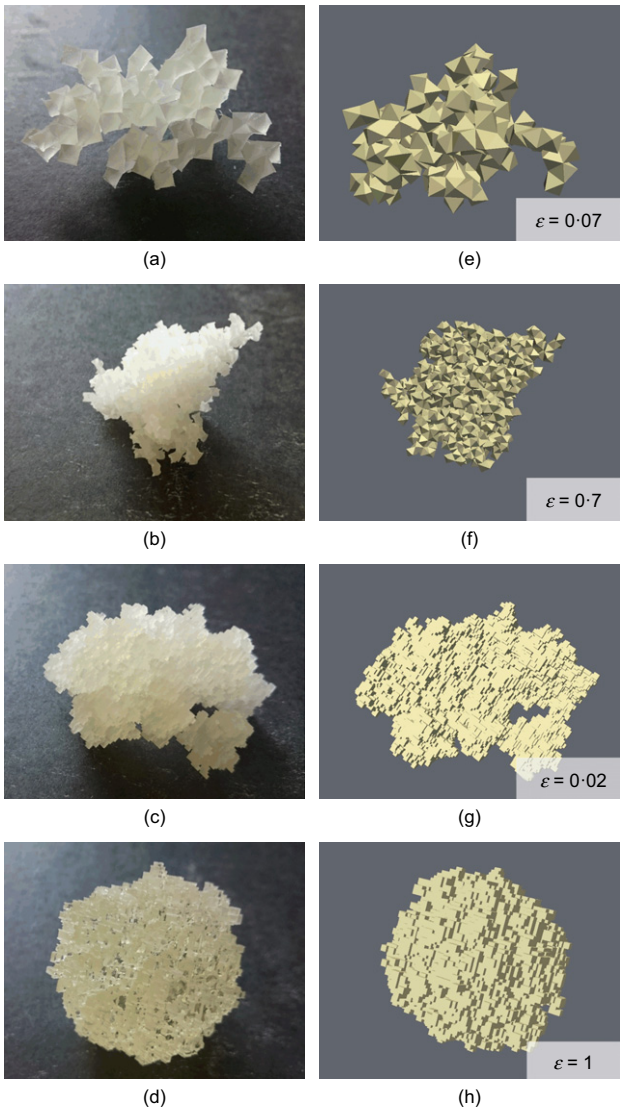

Fig. 9. Comparison of printed (a), (b), (c), (d) and simulated grains (e), (f), (g), (h) obtained by the DPA method

Ahmadi *et al.*, 2011; Sorensen, 2011). The ability to fabricate representative particles of controlled morphology and fractal dimension can facilitate the development and implementation of new integrated experimental and computational studies into the significance of particle morphology on mechanical properties, reactivity and mobility. Moreover DPA algorithms of the type demonstrated here can be adapted to simulate and study the heterogeneous precipitation and growth of particles from solute species through chemical and biological processes (Cölfen, 2003; Chekroun *et al.*, 2004; Hanaor *et al.*, 2012) and also the surface chemistry dependent growth of fractal particles from suspended solid elements through processes of attraction, aggregation, cementation and sedimentation (Kranenburg, 1994; Markus *et al.*, 2015).

In light of Figs 7–9 and the discussion above, Table 1 summarises the relative advantages and drawbacks of the different grain generation methods applied in the current paper.

In the following, the CRI method is adopted for generating bulk quantities of 3D printable grains. Although this method misses some morphological features discussed in Table 1, it has the advantage of allowing input parameters to be obtained from natural geomaterials.

Bulk material response

Grains produced by the CRI method were subjected to geomechanical testing in a triaxial apparatus to investigate their response during compression and shear. Fig. 10 shows a bulk print of 8000 grains of mean diameter 2 mm, which is sufficient for a triaxial specimen with dimensions of 38 mm diameter by 76 mm high. The grains are produced in one print with the same parameters so that they all have the same mean grain diameter, although exhibiting variability in surface roughness owing to the layer-by-layer printing method yielding ridges with 32 μm wavelength perpendicular to the printing direction. The process of printing and etching out this number of particles takes about 1 week. Triaxial tests have been performed using two grain shapes. These have been produced using FDs (0, 0, 0·02) referred to as rough spheres, and FDs (0·15, 0·10, 0·03) referred to as rough and angular, and shown

Table 1. Summary of grain generation methodologies investigated in the present work

FSO	Superimposition of a simulated fractal surface on a 3D geodesic spheroid	
	Benefits	• Reproduction of natural isotropic multi-scale grain surfaces • Grain elongation control by varying highest level wavelength
	Drawbacks	• Extraction of input parameters from real materials is challenging • Absence of smooth facets, angularity and pores • Branching morphologies cannot be simulated • Computationally intensive
CRI	Interpolation and morphing of three 2D contours to generate a 3D surface	
	Benefits	• Input parameters can be readily extracted from 2D grain data • Captures properties of elongation, roughness and irregularities • Appropriate for studying the effect of varying morphology
	Drawbacks	• Absence of smooth facets, angularity and pores • Anisotropic features in the form of parallel ridges • Branching morphologies are not represented
DPA	Controlled assembly of polyhedral elements to yield branching aggregates	
	Benefits	• Reproduction of sediment particles and branching aggregates • Control of aggregate fractality by particle selection exponent • Input parameters can be extracted from particle characterisation
	Drawbacks	• Surface roughness is not meaningfully represented • Cannot simulate solid monolithic particles • Computationally intensive

Fig. 10. Bulk printed granular material with inset showing rough angular particle

in the inset to Fig. 10. Note that the FDs of the rough and angular case are similar to the FDs obtained from the quartz grains, which were used to generate Figs 8(a) and 8(d).

The particles were placed dry, loosely and were tamped to form the triaxial specimens, which were then subjected to a small confining stress before being saturated by percolation of water followed by back pressure saturation. The specimens were then subjected to an effective confining stress of 20 kPa before performing conventional drained shearing tests. Although this confining stress is relatively small from the viewpoint of standard geotechnical tests, the dimensionless ratio of this stress to the stiffness of the printed material is comparable with that for quartz at a confining stress of 1 MPa. Fig. 11(a) shows the evolution of stress ratio and Fig. 11(b) presents the associated volume strains. Values of the void ratios at the start of shearing are indicated on the figures. The results for the rough spheres demonstrate shear behaviour typical of sand. The stress ratio (q/p') of the denser specimen rises to a peak, before reducing, with associated dilation, towards an ultimate state, while the stress ratio of the looser specimen rises gradually and the specimen compresses throughout. An ultimate state with a stress ratio of about 1·5 (friction angle of 37°) is suggested by these responses. This may be compared with an ultimate angle of about 38° indicated by tilt table tests. Two tests are shown for the rough, angular particles and in each the material compressed and the stress ratio rose steadily until the tests were terminated at large strain where the specimens were highly distorted. The slightly wavy responses appear to be material related, as the same methods, equipment and logging rates were used for all tests. The second test was a repeat test using the same particles to confirm the high resistance and also to investigate whether changes in shape of the soft particles could be influencing the shear behaviour. Although a few particles were noticeably changed, it can be seen that the bulk response is not significantly affected. The friction angle implied at the test termination was 55°. While this is unusually high, tilt table tests indicated an ultimate friction angle of 43–48°, significantly higher than for the rough spheres and suggesting that larger strains than can be applied in the triaxial test are required for this angular material to reach an ultimate state. Although the shear responses are typical of geomaterials, during compression time-dependent compressibility was observed as a result of the soft polymer comprising the grains, and further advances in material are needed to fully reproduce geomaterial properties.

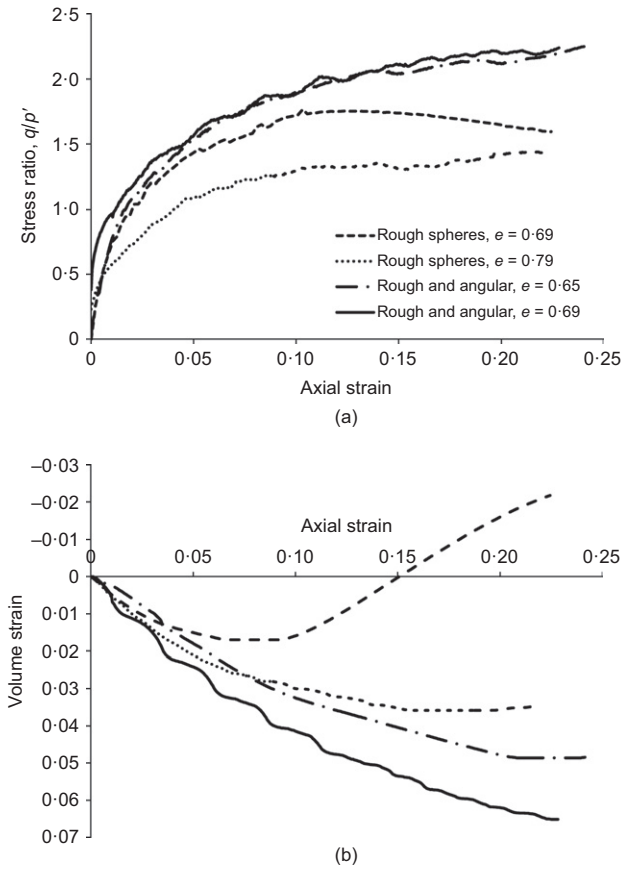

Fig. 11. Triaxial shear behaviour of printed grains: (a) stress ratio, axial strain and (b) volume strain, axial strain

SUMMARY

The generation of geomaterial grain morphologies by techniques such as those described here facilitates the fabrication of surrogate geomaterials by 3D printing. Such materials are utilisable in experimental parametric studies where morphology and material can be decoupled. Here the focus has been on three methods that can be applied to generate realistic and printable grain morphologies. The relative advantages and disadvantages of the three methods were detailed in Table 1; one of these methods, the CRI method, was then employed to generate a large quantity of grains for triaxial testing. These preliminary triaxial tests have confirmed that the printed grains are capable of reproducing aspects of shear behaviour and have shown the significant effect that shape can have on the bulk material behaviour.

The ability of 3D printing techniques to produce a variety of shapes with a single material, as demonstrated here, allows the morphology to be decoupled from the material type. This should enable new areas of research, such as the investigation of the role of grain morphology on the bulk constitutive behaviour, and the role of particle material on the variation of constitutive behaviour while maintaining constant realistic geomorphologies. Currently, the first is restricted by printing resolution, which was 32 μm in the present work, while the second is limited by the available range of printing materials. However, the authors anticipate that rapid progress in 3D printing technology in terms of printing resolution, rapidity and material versatility will address these concerns. The capabilities of ceramic-material printers are continuously increasing and it is anticipated that, rather than just surrogate geomaterials, future research involving the synthesis of artificial mineral geomaterials will be possible. This will enable the fabrication of standardised reference geomaterials for quality control in geotechnical testing with further potential applications as a supplementary material in construction and ground improvement.

NOTATION

A amplitude of surface roughness relative to primitive geodesic radius
D fractal dimension
D_A aggregate fractal dimension
e void ratio at start of triaxial shear test
K scaling factor
L stochastic length parameter
p' mean effective stress
q triaxial shear stress
R grain radius
V true particle volume
Z surface height
γ density of frequencies
ε aggregation exponent
ζ randomised phase angle
θ azimuth in polar coordinates
ρ radius of polar coordinate
ϕ elevation angle
ψ randomised phase angle

REFERENCES

Ahmadi, A., Neyshabouri, M. R., Rouhipour, H. & Asadi, H. (2011). Fractal dimension of soil aggregates as an index of soil erodibility. *J. Hydrol.* **400**, No. 3, 305–311.

Alonso-Marroquin, F. (2008). Spheropolygons: a new method to simulate conservative and dissipative interactions between 2D complex-shaped rigid bodies. *EPL (Europhys. Lett.)* **83**, No. 1, 14001.

Alonso-Marroquín, F. & Wang, Y. (2009). An efficient algorithm for granular dynamics simulations with complex-shaped objects. *Granular Matter* **11**, No. 5, 317–329.

Alonso-Marroquín, F., Mühlhaus, H. B. & Herrmann, H. J. (2008). Micromechanical investigation of granular ratcheting using a discrete model of polygonal particles. *Particuology* **6**, No. 6, 390–403.

Alonso-Marroquín, F., Ramírez-Gómez, Á., González-Montellano, C., Balaam, N., Hanaor, D. A., Flores-Johnson, E., Gan, Y., Chen, S. & Shen, L. (2013). Experimental and numerical determination of mechanical properties of polygonal wood particles and their flow analysis in silos. *Granular Matter* **15**, No. 6, 811–826.

Altuhafi, F., O'sullivan, C. & Cavarretta, I. (2012). Analysis of an image-based method to quantify the size and shape of sand particles. *J. Geotech. Geoenviron. Engng* **139**, No. 8, 1290–1307.

Arasan, S., Akbulut, S. & Hasiloglu, A. S. (2011). The relationship between the fractal dimension and shape properties of particles. *KSCE J. Civ. Engng* **15**, No. 7, 1219–1225.

Ausloos, M. & Berman, D. (1985). A multivariate Weierstrass-Mandelbrot function. *Proc. R. Soc. Lond. A. Math. Phys. Sci.* **400**, No. 1819, 331–350.

Babadagli, T. & Develi, K. (2003). Fractal characteristics of rocks fractured under tension. *Theor. Appl. Fracture Mech.* **39**, No. 1, 73–88.

Barrett, P. (1980). The shape of rock particles, a critical review. *Sedimentology* **27**, No. 3, 291–303.

Blott, S. J. & Pye, K. (2008). Particle shape: a review and new methods of characterization and classification. *Sedimentology* **55**, No. 1, 31–63.

Bowman, E. T., Soga, K. & Drummond, W. (2001). Particle shape characterisation using Fourier descriptor analysis. *Géotechnique* **51**, No. 6, 545–554, http://dx.doi.org/10.1680/geot.2001.51.6.545.

Brantley, S. L., White, A. F. & Hodson, M. (1999). Surface area of primary silicate minerals. In *Growth, dissolution and pattern formation in geosystems* (eds B. Jamtveit and P. Meakin), pp. 291–326. Amsterdam, the Netherlands: Springer.

Brisard, S., Chae, R. S., Bihannic, I., Michot, L., Guttmann, P., Thieme, J., Schneider, G., Monteiro, P. J. & Levitz, P. (2012). Morphological quantification of hierarchical geomaterials by X-ray nano-CT bridges the gap from nano to micro length scales. *Am. Mineralogist* **97**, No. 2–3, 480–483.

Buzio, R., Boragno, C., Biscarini, F., De Mongeot, F. B. & Valbusa, U. (2003). The contact mechanics of fractal surfaces. *Nature Mater.* **2**, No. 4, 233–237.

Cavarretta, I., Coop, M. & O'Sullivan, C. (2010). The influence of particle characteristics on the behaviour of coarse grained soils. *Géotechnique* **60**, No. 6, 413–423, http://dx.doi.org/10.1680/geot.2010.60.6.413.

Chekroun, K. B., Rodríguez-Navarro, C., González-Muñoz, M. T., Arias, J. M., Cultrone, G. & Rodríguez-Gallego, M. (2004). Precipitation and growth morphology of calcium carbonate induced by *Myxococcus xanthus*: implications for recognition of bacterial carbonates. *J. Sedimentary Res.* **74**, No. 6, 868–876.

Cho, G. C., Dodds, J. & Santamarina, J. C. (2006). Particle shape effects on packing density, ss, and strength: natural and crushed sands. *J. Geotech. Geoenviron. Engng* **132**, No. 5, 591–602.

Ciavarella, M., Delfine, V. & Demelio, V. (2006). A new 2D asperity model with interaction for studying the contact of multiscale rough random profiles. *Wear* **261**, No. 5, 556–567.

Ciavarella, M., Greenwood, J. & Paggi, M. (2008). Inclusion of 'interaction' in the Greenwood and Williamson contact theory. *Wear* **265**, No. 5, 729–734.

Cölfen, H. (2003). Precipitation of carbonates: recent progress in controlled production of complex shapes. *Curr. Opinion Colloid Interface Sci.* **8**, No. 1, 23–31.

Cundall, P. & Strack, O. (1979). A discrete numerical model for granular assemblies. *Géotechnique* **29**, No. 1, 47–65, http://dx.doi.org/10.1680/geot.1979.29.1.47.

Ehrlich, R. & Weinberg, B. (1970). An exact method for characterization of grain shape. *J. Sedimentary Res.* **40**, No. 1, 205–212.

Erlebacher, J., Searson, P. & Sieradzki, K. (1993). Computer simulations of dense-branching patterns. *Phys. Rev. Lett.* **71**, No. 20, 3311.

Fraysse, N., Thomé, H. & Petit, L. (1999). Humidity effects on the stability of a sandpile. *Eur. Phys. J. B – Condensed Matter and Complex Systems* **11**, No. 4, 615–619.

Gastaldi, A. & Vanni, M. (2011). The distribution of stresses in rigid fractal-like aggregates in a uniform flow field. *J. Colloid Interface Sci.* **357**, No. 1, 18–30.

Hanaor, D., Chironi, I., Karatchevtseva, I., Triani, G. & Sorrell, C. (2012). Single and mixed phase TiO_2 powders prepared by excess hydrolysis of titanium alkoxide. *Adv. Appl. Ceramics* **111**, No. 3, 149–158.

Hanaor, D. A., Gan, Y. & Einav, I. (2013). Effects of surface structure deformation on static friction at fractal interfaces. *Géotechnique Lett.* **3**, No. 2, 52–58.

Hanaor, D. A., Gan, Y. & Einav, I. (2015). Contact mechanics of fractal surfaces by spline assisted discretization. *Int. J. Solids Structs* **59**, 121–131.

Hanaor, D. A. H., Ghadiri, M., Chrzanowski, W. & Gan, Y. (2014). Scalable surface area characterisation by electrokinetic analysis of complex anion adsorption. *Langmuir* **30**, No. 50, 15143–15152.

Komvopoulos, K. (2008). Effects of multi-scale roughness and frictional heating on solid body contact deformation. *Comptes Rendus Mécanique* **336**, No. 1, 149–162.

Kranenburg, C. (1994). The fractal structure of cohesive sediment aggregates. *Estuarine, Coastal and Shelf Sci.* **39**, No. 6, 451–460.

Krumbein, W. C. & Sloss, L. L. (1951). Stratigraphy and sedimentation. *Soil Sci.* **71**, No. 5, 401.

Langston, P., Ai, J. & Yu, H. S. (2013). Simple shear in 3D DEM polyhedral particles and in a simplified 2D continuum model. *Granular Matter* **15**, No. 5, 595–606.

Liao, C. W., Yu, J. H. & Tarng, Y. S. (2010). On-line full scan inspection of particle size and shape using digital image processing. *Particuology* **8**, No. 3, 286–292.

Maggi, F. & Winterwerp, J. (2004). Method for computing the three-dimensional capacity dimension from two-dimensional projections of fractal aggregates. *Phys. Rev. E* **69**, No. 1, 011405.

Markus, A., Parsons, J., Roex, E., De Voogt, P. & Laane, R. (2015). Modeling aggregation and sedimentation of nanoparticles in the aquatic environment. *Sci. Total Environ.* **506**, 323–329.

Matsushima, T., Saomoto, H., Matsumoto, M., Toda, K. & Yamada, Y. (2003). Discrete element simulation of an assembly of irregularly-shaped grains: quantitative comparison with experiments. *Proceedings of the 16th ASCE engineering*

mechanics conference, Seattle, WA, USA. Reston, VA, USA: American Society of Civil Engineers (CD-ROM).

Miskin, M. Z. & Jaeger, H. M. (2013). Adapting granular materials through artificial evolution. *Nature Mater.* **12**, No. 4, 326–331.

Mollon, G. & Zhao, J. (2012). Fourier–Voronoi-based generation of realistic samples for discrete modelling of granular materials. *Granular Matter* **14**, No. 5, 621–638.

Mollon, G. & Zhao, J. (2013a). Generating realistic 3D sand particles using Fourier descriptors. *Granular Matter* **15**, No. 1, 95–108.

Mollon, G. & Zhao, J. (2013b). The influence of particle shape on granular hopper flow. In *Powders and grains 2013: proceedings of the 7th international conference on micromechanics of granular media* (eds A. Yu, K. Dong, R. Yang and S. Luding), pp. 690–693. Melville, NY, USA: AIP Publishing.

Mollon, G. & Zhao, J. (2014). 3D generation of realistic granular samples based on random fields theory and Fourier shape descriptors. *Comput. Methods Appl. Mech. Engng.* **279**, 46–65.

Natalini, P., Patrizi, R. & Ricci, P. E. (2008). The Dirichlet problem for the Laplace equation in a starlike domain of a Riemann surface. *Numer. Algorithms* **49**, No. 1–4, 299–313.

Pena, A., Garcia-Rojo, R. & Herrmann, H. (2007). Influence of particle shape on sheared dense granular media. *Granular Matter* **9**, No. 3–4, 279–291.

Persson, A. S. & Frenning, G. (2012). An experimental evaluation of the accuracy to simulate granule bed compression using the discrete element method. *Powder Technol.* **219**, 249–256.

Pourghahramani, P. & Forssberg, E. (2005). Review of applied particle shape descriptors and produced particle shapes in grinding environments. Part I: particle shape descriptors. *Miner. Processing Extractive Metall. Rev.* **26**, No. 2, 145–166.

Qin, J., Zhong, D., Wang, G. & Ng, S. L. (2013). Influence of particle shape on surface roughness: dissimilar morphological structures formed by man-made and natural gravels. *Geomorphology* **190**, 16–26.

Robertson, M. (1936). Analytic functions star-like in one direction. *Am. J. Math.* **58**, No. 3, 465–472.

Russel, A. (2014). How water retention in fractal soils depends on particle and pore sizes, shapes, volumes and surface areas. *Géotechnique* **64**, No. 5, 379–390, http://dx.doi.org/10.1680/geot.13.P.165.

Salot, C., Gotteland, P. & Villard, P. (2009). Influence of relative density on granular materials behavior: DEM simulations of triaxial tests. *Granular Matter* **11**, No. 4, 221–236.

Scheel, M., Seemann, R., Brinkmann, M., Di Michiel, M., Sheppard, A., Breidenbach, B. & Herminghaus, S. (2008). Morphological clues to wet granular pile stability. *Nature Mater.* **7**, No. 3, 189–193.

Schmid, H. J., Tejwani, S., Artelt, C. & Peukert, W. (2004). Monte Carlo simulation of aggregate morphology for simultaneous coagulation and sintering. *J. Nanoparticle Res.* **6**, No. 6, 613–626.

Sorensen, C. (2011). The mobility of fractal aggregates: a review. *Aerosol Sci. Technol.* **45**, No. 7, 765–779.

Tang, P. & Raper, J. A. (2002). Modelling the settling behaviour of fractal aggregates–a review. *Powder Technol.* **123**, No. 2, 114–125.

Tang, P., Greenwood, J. & Raper, J. A. (2002). A model to describe the settling behavior of fractal aggregates. *J. Colloid Interface Sci.* **247**, No. 1, 210–219.

Tang, P., Chew, N. Y., Chan, H. K. & Raper, J. A. (2003). Limitation of determination of surface fractal dimension using N2 adsorption isotherms and modified Frenkel-Halsey-Hill theory. *Langmuir* **19**, No. 7, 2632–2638.

Tang, S., Ma, Y. & Shiu, C. (2001). Modelling the mechanical strength of fractal aggregates. *Colloids Surf. A: Physicochem. Engng Aspects* **180**, No. 1, 7–16.

Tarnawski, V. R., Momose, T., Leong, W., Bovesecchi, G. & Coppa, P. (2009). Thermal conductivity of standard sands. Part I. Dry-state conditions. *Int. J. Thermophysics* **30**, No. 3, 949–968.

Thomas, M., Wiltshire, R. & Williams, A. (1995). The use of Fourier descriptors in the classification of particle shape. *Sedimentology* **42**, No. 4, 635–645.

Thomas, P. A. & Bray, J. D. (1999). Capturing nonspherical shape of granular media with disk clusters. *J. Geotech. Geoenviron. Engng* **125**, No. 3, 169–178.

Torquato, S. & Jiao, Y. (2009a). Dense packings of polyhedra: Platonic and Archimedean solids. *Phys. Rev. E* **80**, No. 4, 041104.

Torquato, S. & Jiao, Y. (2009b). Dense packings of the Platonic and Archimedean solids. *Nature* **460**, No. 7257, 876–879.

Yan, W. & Komvopoulos, K. (1998). Contact analysis of elastic-plastic fractal surfaces. *J. Appl. Phys.* **84**, No. 7, 3617–3624.